RSC Advances

PAPER

View Article Online
View Journal | View Issue

Cite this: *RSC Adv.*, 2026, **16**, 9440

Injectable ε-poly-lysine/hyaluronic acid hydrogel for targeted prevention of cardiovascular implantable electronic device pocket infections

Jin-e Liu,†[a] Zikang Cheng,†[a] Peixu Zhao,[a] Yanfei Wu,[a] Lingjuan Zhu,[ab] Chao Yu,[ab] Wei Zhou,[ab] Tao Wang,[ab] Xiaoshu Cheng,[ab] Quanbin Dong *[ab] and Huihui Bao *[ab]

Cardiovascular implantable electronic device (CIED) pocket infections represent a grave threat to the survival quality and life safety of patients with cardiovascular diseases, while also imposing a substantial economic burden on healthcare systems. However, the efficacy of current approaches employed for preventing CIED pocket infections remains suboptimal. In this study, an injectable antibacterial hydrogel was successfully constructed by physically crosslinking carboxyl groups on the surface of hyaluronic acid microspheres (HAG) with amino groups on poly-L-lysine (PLL). The developed HAG/PLL hydrogel exhibited not only non-toxicity toward L929 cells but also excellent cytocompatibility, accompanied by a low hemolysis rate when tested with red blood cells. Furthermore, *in vivo* experiments demonstrated that the HAG/PLL hydrogel showed no toxicity to vital organs (including the heart, liver, and kidney) as well as local tissues at the implantation site. Moreover, the HAG/PLL hydrogel effectively eliminated *Staphylococcus aureus* and *Escherichia coli* bacteria by promoting ROS production, thereby inducing bacterial cell membrane disruption. In conclusion, HAG/PLL hydrogels were simply and conveniently prepared and showed considerable potential in the prevention of CIED infections owing to their excellent biocompatibility and antimicrobial properties.

Received 5th November 2025
Accepted 9th February 2026

DOI: 10.1039/d5ra08511j

rsc.li/rsc-advances

1. Backgrounds

Rapid advances in cardiac electrophysiology have led to a significant rise in the number of patients receiving cardiovascular implantable electronic devices (CIEDs).[1] Concurrently, there has been a significant increase in the incidence of CIED pocket infections.[2,3] Characterized by substantial healthcare costs and high morbidity and mortality rates, CIED-associated infections have emerged as a major challenge in the clinical practice setting and impose a substantial economic burden on both the national healthcare system and individual patients.[4] Consequently, the prevention of such infections holds significant implications and societal value.[5,6]

Epidemiological studies have established *Staphylococcus aureus* and *Escherichia coli* as the predominant pathogens in CIED-associated infections, with a high prevalence of coagulase-negative and oxacillin sensitive *S. aureus* strains, which are responsible for approximately 70% of infections.[7–9] According to an earlier study, among all cardiac device infections, pocket infections pose the greatest diagnostic challenge.[10] Current clinical guidelines recommend the use of preoperative prophylactic intravenous antibiotics as the primary preventive measure against CIED pocket infections.[4,11] However, due to the avascular nature and poor tissue perfusion of the pocket, intravenous antibiotics may not be effective in preventing infections.[8] Thus, the development of medical materials with inherent antimicrobial properties that can be implanted directly into surgical incisions has garnered extensive attention, offering innovative solutions to combat CIED-associated infections and antibiotic resistance. The AigisRx antimicrobial envelope, a high-polymer blend containing minocycline and rifampicin, has been pioneered to mitigate device-associated infections by regulating the release of antibiotics.[12] Numerous studies have demonstrated that this envelope significantly decreases the risk of CIED infections and has been approved for clinical use in both the USA and Canada.[12–16] Plasma-based material (PBM), a bioactive substance derived from a mixture of allogeneic plasma and platelets, serves as a reliable antibiotic delivery vehicle. Indeed, PBM, loaded with minocycline and rifampicin, has been documented to effectively eliminate bacteria in a rabbit pacemaker infection

[a]*Department of Cardiovascular Medicine, Center for Prevention and Treatment of Cardiovascular Diseases, Jiangxi Provincial Cardiovascular Disease Clinical Medical Research Center, the Second Affiliated Hospital, Jiangxi Medical College, Nanchang University, No. 1 Minde Road, Nanchang, Jiangxi, China. E-mail: huihui_bao77@126.com; dongquanbin@163.com*

[b]*The Second Affiliated Hospital, Jiangxi Medical College, Nanchang University, Nanchang, Jiangxi, China*

† Jin-e Liu and Zikang Cheng contributed equally to this work.

model.[17] However, the increasing challenge of antibiotic resistance, exacerbated by the misuse of antibiotics and the formation of biofilms by bacteria on the surfaces of implanted devices, has become a critical concern.[18] While both the AigisRx antimicrobial mesh and PBM are engineered to prevent CIED pocket infections *via* the sustained release of antibiotics, this approach also carries the potential to facilitate the development of drug resistance.

Thus, there is an urgent need to develop novel antibiotics or explore non-antibiotic alternatives, as well as to innovate drug administration methods to enhance the bioavailability of antimicrobial therapies and delay the onset of bacterial resistance. Various novel antimicrobial materials have been developed, encompassing antimicrobial peptides,[19] organometallic ions,[20] and bio-based antimicrobial materials,[21] which effectively minimize the risk of hospital-acquired infections. Notably, these materials exhibit broad potential for application across various fields, particularly in medicine.[22]

ε-Poly-lysine (ε-PLL) is a homopolymer composed of L-lysine residues derived from the essential amino acid L-lysine. It is formed by the condensation of the ε-amino group of L-lysine with the α-carboxylate group, creating an ε-amide bond. ε-PLL is heat-resistant, has a broad pH tolerance, exhibits low toxicity and high safety, and possesses excellent water solubility.[23,24] In its highly polymerized polyvalent cationic form, ε-PLL can disrupt the cell membrane structure of microorganisms through electrostatic interactions, thereby exerting broad-spectrum bactericidal effects.[25,26] Indeed, several studies have corroborated the potent bactericidal effect of ε-PLL against both Gram-positive and Gram-negative bacteria, including *S. aureus* and *E. coli*.[27,28] However, as a small molecule antimicrobial peptide, ε-PLL is highly unstable *in vivo* and can be hydrolyzed by various enzymes within minutes,[29] thereby restricting its ability to provide sustained *in vivo* antimicrobial efficacy when used alone.

Hyaluronic acid (HA) is renowned for its excellent biocompatibility and biodegradability.[30–32] HA not only mitigates inflammatory responses and scar formation but also facilitates the migration and repair of epithelial cells, thereby promoting wound healing and tissue regeneration. These properties have led to its widespread application in biomedicine.[33–35] Of note, HA can form a network with water molecules through hydrogen bonding involving the carboxyl and amino groups in its structure. Consequently, HA with a high molecular weight exhibits greater stability, viscosity, and viscoelasticity.[36] The ionic strength, pH, and temperature of the solution can influence the mobility and degradability of HA, factors that must be considered when formulating HA-based biomaterials.[37] Additionally, previous investigations have demonstrated that HA can modulate intracellular signaling by binding to CD44 receptors on the surfaces of monocytes and granulocytes, thereby exerting anti-inflammatory and pro-angiogenic effects that promote the

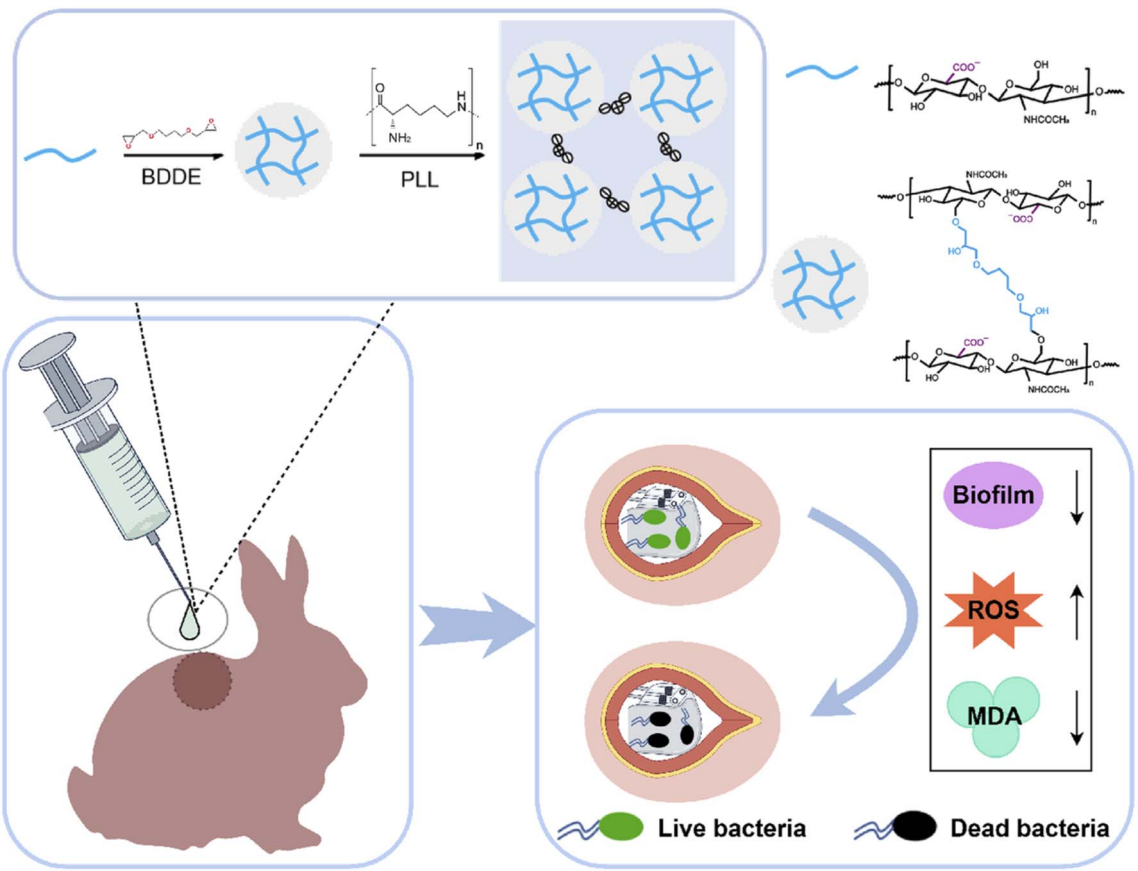

Scheme 1 The HAG/PLL hydrogels synthesis and application.

healing of damaged skin.[38,39] Various HA-based wound dressings, such as sponges,[40] hydrogels,[41] electro-spun membranes,[42] and fillers,[43,44] have been utilized in clinical practice and show significant potential for applications in bioengineering.

To effectively prevent CIED pocket infections, an injectable antimicrobial hydrogel was developed by integrating hyaluronic acid microspheres (HAG) with ε-PLL (Scheme 1). In this antibacterial system, the HA scaffold is pre-crosslinked with 1,4-butanediol diglycidyl ether (BDDE) to form an HA hydrogel with a low crosslinking density, which prevents rapid degradation while preserving fluidity. Following this, the carboxyl groups of HAG electrostatically interact with the amino groups on poly-L-lysine (PLL), whilst the milled micro-hydrogel is further reinforced through physical crosslinking, resulting in the hybrid hydrogel (HAG/PLL). Characterized by superior physicochemical properties, injectability, and self-healing capabilities, the HAG/PLL hydrogel can be easily and uniformly administered within the CIED pocket. Moreover, its outstanding antimicrobial capacity can effectively protect against potential bacterial infections, while its excellent biocompatibility limits foreign body responses. Overall, the findings of this study suggest that the injectable antimicrobial hydrogel holds significant implications for the prevention of CIED infections owing to its remarkable antimicrobial properties and biocompatibility.[45–48]

2. Materials and methods

2.1 Materials

HA (1.48×10^3 kDa) was purchased from Shanxi Dasheng Science and Technology Company. PLL (Mw: 3500–4500 kDa) was procured from Zhengzhou Forida Company. Bacteria were sourced from the American Typical Culture Collection (ATCC, USA), and L929 mouse fibroblasts were kindly provided by the Chinese Academy of Sciences Stem Cell Bank. Live/dead viability/cytotoxicity kit (L3224), live/dead BacLight Bacterial Viability Kit (L7012), phosphate-buffered saline (PBS), Dulbecco's modified Eagle's medium (DMEM), fetal bovine serum (FBS), nutrient agar, and tryptic soy broth (TSB) were acquired from Thermo Fisher Scientific (USA). *N*-Acetylcysteine (NAC) was purchased from sigma. Rifampicin (RFP) was purchased from SparkJade. Other reagents were used directly without purification.

2.2 Synthesis of HA hydrogels

The method used to synthesize HA hydrogels was based on a previous study.[49] Initially, 10 g of HA powder was gradually added to 100 mL of 1 mol L^{-1} NaOH solution while stirring, and then 1 mL BDDE were introduced. The resulting mixture was stirred at room temperature until homogeneous. Next, it was heated and stirred at 35 °C for 3 h to ensure complete crosslinking, resulting in cross-linked sodium hyaluronate. The obtained cross-linked sodium hyaluronate was dialyzed to discard NaOH and BDDE, following which residual BDDE was removed *via* ethanol reprecipitation. Finally, HA hydrogel powder with consistent particle sizes were obtained *via* lyophilization, milling, and sieving. The diameter of HA hydrogel powder was 0.74 μm.

2.3 Preparation of HAG and HAG/PLL hydrogels

To prepare HAG hydrogel, 0.06 g of HA hydrogel powder was dissolved in 1 mL PBS. Separately, 0.10 g of PLL powder was dissolved in 1 mL PBS to obtain the PLL solution. Then, the HAG hydrogel and PLL solution were mixed in a 1 : 1 volume ratio, and the pH was adjusted to 8 by adding NaOH solution. The carboxyl group with a negative charge on HA interacts electrostatically with the amino group with a positive charge on PLL. Finally, the injectable antimicrobial hydrogel was formed.

2.4 Rheology measurements of the hydrogels

The viscoelastic and self-healing characteristics of the hydrogels were assessed using a HAAKE MARS III rheometer. Briefly, hydrogels were carefully positioned between the rheometer's plates. To determine the energy storage modulus (G') and loss modulus (G'') of the hydrogels, strain tests were conducted at a physiological temperature of 37 °C and a frequency of 1 Hz. Furthermore, the thixotropic behavior of the HAG/PLL hydrogel was assessed using a dynamic rheometer over the whole range or alternate strain amplitudes of 0.1% and 1000% at a constant frequency (1 Hz).

2.5 *In vitro* PLL release measurement

Fluorescein isothiocyanate (FITC) was covalently conjugated to PLL, and the absorption standard curve of PLL-FITC was established *via* quantitative detection with a microplate reader. Briefly, 200 μL of HAG-PLL-FITC hydrogels was transferred into EP tubes, with the initial weight of each tube recorded. Subsequently, 2 mL of PBS (pH = 7.4 or 5.0) was added to each tube, and the tubes were incubated at 37 °C. At predetermined time points, 1 mL of the supernatant was collected from each tube, and the fluorescence absorbance of the supernatant at 495 nm was measured using a microplate reader. The concentration of released PLL-FITC was calculated according to the regression equation of the pre-established standard curve, and the cumulative release rate of PLL-FITC at each time point was further determined based on the calculated concentration.

2.6 *In vivo* degradation assay

The *in vivo* degradation of the HAG/PLL hydrogels was assessed in a Sprague-Dawley (SD) rat model using fluorescence imaging. FITC-labeled hydrogels (100 μL) were injected into a dorsal subcutaneous pouch in SD rats. The retention and morphological integrity of the fluorescent hydrogels were monitored *in vivo* under ultraviolet light at predetermined time points to visually track the degradation process.

2.7 Morphological analysis

The prepared HAG and HAG/PLL hydrogels were stored at −21 °C overnight before being freeze-dried in a lyophilizer for 48 hours. The freeze-dried hydrogels were subsequently frozen in liquid nitrogen. Selected surfaces of the samples were sputter-

coated with gold, and their morphology was examined using scanning electron microscopy (SEM, Model S-4800, HITACHI) at an acceleration voltage of 5 kV.

2.8 Biocompatibility of hydrogel *in vitro*

2.8.1 CCK8 cytotoxicity assay. The biocompatibility of HAG/PLL hydrogels with L929 mouse fibroblasts was assessed using the CCK-8 assay kit. L929 cells were seeded into 96-well plates at a density of 3×10^4 cells per mL and allowed to adhere overnight in a humidified incubator at 37 °C with 5% CO_2. Subsequently, the original medium was discarded, and the cells were treated with PLL solution of different concentrations for 24 hours and the cells were treated with HAG/PLL hydrogel for 24 hours and 72 hours respectively. As a control, the cells were cultured with DMEM modified Eagle Medium containing 10% fetal bovine serum. Then 100 μL of DMEM supplemented with 10 μL of CCK-8 reagent was introduced into each well. The plates were subsequently incubated for 2 hours. Lastly, absorbance (OD) was recorded at 450 nm using a microplate reader to quantify cell viability.

2.8.2 Staining of living and dead cells. The biocompatibility of the hydrogel was evaluated using a live/dead assay kit. L929 cells were cultured in 24-well plates at two different seeding densities, 1×10^4 cells per mL and 2×10^4 cells per mL. The cells were then exposed to the growth medium extract of the hydrogel as well as to DMEM for 24 and 72 hours, respectively. Following incubation, each sample was stained with a solution containing calcein AM (0.5 μL mL^{-1}) to label live cells and ethidium homodimer-1 (EthD-1, 2 μL mL^{-1}) to label dead cells. Afterward, the cells were incubated at 37 °C for 20 minutes to allow for the penetration and binding of the dyes. The stained cells were subsequently visualized under an inverted fluorescence microscope to distinguish live from dead cells based on their fluorescence signatures.

2.8.3 Evaluation of hemocompatibility. In addition, the *in vitro* biocompatibility of the HAG/PLL hydrogel was determined by evaluating its *in vitro* hemocompatibility. Whole blood was collected from SD rats. Erythrocytes were collected through centrifugation at 1500 rpm for 15 min, washed 3 times with PBS, and resuspended in PBS. Prepare red blood cells into a 4% red blood cell solution for substitution; Take a 1 mL EP tube, add 1 mL of 4% red blood cell solution, centrifuge at 3000 rpm for 10 minutes, and discard the supernatant. Add PBS to the hydrogel prepared with different concentrations of PLL at a ratio of 10 : 1, and after 24 hours of extraction, 1 mL of hydrogel extract was taken and added to an EP tube containing red blood cell sediment. Triton X-100 and PBS were used as positive and negative controls, respectively. After mixing the above solution evenly, place it in a 37 °C oven for 3 hours, then centrifuge it at 3000 rpm for 10 minutes, observe whether there is hemolysis in the supernatant, the absorbance of the supernatant was measured at 540 nm.

2.9 *In vivo* biocompatibility of hydrogel

All animal procedures were performed in accordance with the Guidelines for Care and Use of Laboratory Animals of the National Natural Science Foundation of China and approved by the Animal Ethics Committee of the National Natural Science Foundation of China. Male SD rats, weighing between 250–350 grams, were randomly assigned to either the control group or the experimental group. A surgical incision of approximately 3 cm was made using a scalpel to dissect the fascia and create a pouch. Rats in the control group received an injection of phosphate-buffered saline (PBS), whereas those in the experimental group were injected with the HAG/PLL hydrogel at the surgical site. During the study, tissue, heart, liver, kidney, and blood samples were harvested from the vicinity of the injection site at two predefined time points: the 7th and 30th days post-injection. Tissue samples were then stained with hematoxylin and eosin (H&E) to evaluate the local inflammatory response. Additionally, blood samples were collected from rats for a comprehensive assessment of routine blood parameters, as well as liver and kidney function.

2.10 Assessment of antimicrobial properties *in vitro*

In this study, the antimicrobial properties of HAG/PLL hydrogel *in vitro* were evaluated using antibacterial assays, including the ring of inhibition, colony counting assay, fluorescence staining of live/dead bacteria, and electron microscopic morphology analysis of Gram-negative and Gram-positive bacteria.

HAG/PLL hydrogels were prepared with different PLL levels and co-cultured with infection-causing bacteria G^+ (*S. aureus*) and G^- (*E. coli*) to investigate the effect of PLL content on the antibacterial effect. PBS and HAG/PLL hydrogels with varying PLL contents (0 wt%, 1 wt%, 3 wt%, 5 wt%, and 10 wt%) were co-cultured with bacteria (100 μL, 1×10^7 CFU mL^{-1}) for 24 hours. Subsequently, the inhibition zone diameters for each group were measured and subjected to statistical analysis. All experiments were performed in triplicate.

100 μL bacterial suspension with a concentration of 1×10^7 CFU mL^{-1} was collected and co cultured with 1 mL PBS, HAG solution, PLL solution, and HAG/PLL hydrogel extract respectively. After 24 hours, the bacteria were collected centrifugally and inoculated onto LB medium. After 24 hours, the bacterial colony growth was observed and quantitative analysis was carried out. The experiment was repeated three times.

A layer of HAG/PLL hydrogel was evenly applied to the surface of peptide slices in the experimental group while control peptide slices remained untreated. A 100 μL aliquot of bacterial suspension, with a concentration of 1×10^7 CFU mL^{-1}, was added dropwise to both experimental and control peptide slices and subsequently incubated at 37 °C for 24 hours before being removed. Each peptide slice was subsequently soaked in sterile PBS and placed in an ultrasonic water bath at 37 °C for 1 minute to dislodge any attached bacteria. After the suspensions were diluted 10 000-fold and uniformly spread onto nutrient agar plates, the plates were incubated at 37 °C for 24 hours. The plates were then observed and photographed. Additionally, 100 μL of a 1×10^7 CFU mL^{-1} bacterial suspension was transferred onto the surfaces of blank wells and HAG/PLL hydrogel, respectively, and incubated at 37 °C for 1 hour. Following this, 100 μL of a bacterial live/dead staining working solution

containing SYTO9 and PI was added, and the mixture was incubated at 37 °C for 20 minutes. The staining solution was then removed, and the residual bacterial staining solution was rinsed with PBS three times. Finally, the samples were observed and photographed under a fluorescence microscope.

In addition, the HAG/PLL hydrogel was co-cultured with *S. aureus* and *E. coli*, following which the morphology of adherent bacteria on the hydrogel was observed using SEM.

2.11 Assessment of antimicrobial properties *in vivo*

To evaluate the in *vivo* antimicrobial performance of HAG/PLL hydrogels, the New Zealand rabbit pocket infection model was constructed. In short, New Zealand rabbits were shaved and disinfected after anesthesia, and pacemakers and 100 μL 1×10^9 CFU mL^{-1} *S. aureus* bacterial solution were implanted in the subcutaneous pouch of rabbits to simulate the CIED pocket. Subsequently, 200 μL HAG/PLL hydrogel was added to the hydrogel group, 200 μL PBS was added to the model group, and 200 μL RFP injection was added to the RFS group. The control group only had pacemakers implanted and did not require infusion. Immediately suture the wound after each group has completed the treatment. After 7 days, observe the infection of the pocket and remove the pacemaker for live/dead bacterial staining. Collect rabbit blood to detect inflammatory indicators and perform H&E staining and immunohistochemical analysis on the pocket tissue.

2.12 Exploration of potential antimicrobial mechanisms in HAG/PLL hydrogels

To explore the specific antimicrobial mechanism of HAG/PLL hydrogels, bacterial reactive oxygen species assays, bacterial MDA content determination, and biofilm formation assays were conducted.

To begin, were used to treat 1 mL of 1×10^8 CFU mL^{-1} *S. aureus* bacterial solution was treated with 1 mL of HAG/PLL hydrogel extract, PBS, PLL solution, NAC, and NAC + HAG/PLL hydrogel extract for 1 h, respectively. Then the organisms were collected *via* centrifugation, suspended in diluted DCFH-DA, and incubated at 37 °C for 20 min. Every 3–5 minutes, the mixture was mixed. After incubation, DCFH-DA was removed through centrifugation, washed three times with serum-free medium, and then transferred into 24-well plates, and bacterial reactive oxygen species levels were visualized using fluorescence microscopy.

S. aureus and *E. coli* were harvested by centrifugation, and each bacterial strain was individually resuspended in broth, HAG, PLL solution, and hydrogel extract to a final concentration of 1×10^8 CFU mL^{-1}. The bacterial suspensions were then inoculated into 24-well plates, with three wells per group, which were incubated in a 5% CO_2 incubator at 37 °C for 24 hours to observe biofilm formation. After incubation, the biofilms were fixed with 70% methanol for 30 minutes, and the plates were air-dried at 37 °C for 30 minutes. Afterward, a 1% crystal violet staining solution was added, and the plates were incubated at room temperature for 5 minutes. The staining solution was then aspirated, and the wells were washed three times with PBS. Finally, the stained biofilms were photographed under a microscope, and the experimental results were recorded.

S. aureus was cultured to a concentration of 1×10^9 CFU mL^{-1} and then treated with HAG/PLL hydrogel extracts or PBS for 1 hour at 37 °C. After the treatment, bacterial were harvested by centrifugation, rinsed three times with sterile PBS to remove residual extracts, and lysed using a mixture of western blot and IP histiocyte lysis buffer combined with ultrasonic disruption. Subsequently, the bacterial lysate was centrifuged at 12 000×*g* for 10 minutes at 4 °C to collect the supernatant, and the protein concentration of the supernatant was determined using a BCA protein concentration assay kit according to the manufacturer's instructions. For malondialdehyde (MDA) quantification, the supernatant was mixed with the MDA assay working solution, and the absorbance was measured at 532 nm using a microplate reader. MDA, a well-recognized indicator of oxidative stress, was quantified based on the measured absorbance values.

2.13 Statistical analyses

All data are shown as mean ± standard deviation (SD). Experimental data were analyzed using one-way analysis of variance (ANOVA) and Tukey *post hoc* analysis. A p-value of <0.05 was considered statistically significant.

3. Results and discussion

3.1 Characterization of the HAG/PLL hydrogels

To screen for the optimal PLL content, the rheological properties of HAG/PLL hydrogels were characterized at 37 °C using a HAAKE MARS III advanced rotational rheometer. Under a constant frequency (1 Hz) and strain amplitude (1%). As illustrated in Fig. 1A, the storage modulus (G') of both HAG and HAG/PLL hydrogels remained consistently higher than the loss modulus (G''), indicating that both hydrogel formulations existed in a gel state. Moreover, G' of HAG/PLL hydrogels was observed to be higher than that of pure HAG hydrogels, which is ascribed to the electrostatic interactions arising from protonated amino groups ($-NH_3^+$) of PLL and deprotonated carboxyl groups ($-COO^-$) on the HAG surface. Notably, as the PLL concentration increased, G' exhibited a gradual decline. The incorporation of PLL may alters the pH value of the gel system, which in turn affects the ionization states, molecular conformations, and interaction modes of HAG and PLL, thereby influencing the modulus of the hydrogel. As shown in Fig. 1B, the HAG/PLL hydrogels could be injected *via* a26 G (ϕ 0.46 mm) syringe needle. As illustrated in Fig. 1C and D, the HAG/PLL hydrogel was in a completely fragmented state under a 1000% strain rate at 37 °C, as determined by a scanning test of strain amplitude in the range of 0.1 to 1000% at a frequency of 1 Hz. Consequently, two strain rates, 1% and 1000%, were selected for the cyclic transition test. Interestingly, the hydrogel repeatedly shattered at a 1000% strain rate and recovered at a 1% strain rate. The HAG/PLL hydrogel forms a polyelectrolyte complex network primarily through electrostatic interactions. The formation process of the hydrogel is a dynamic equilibrium

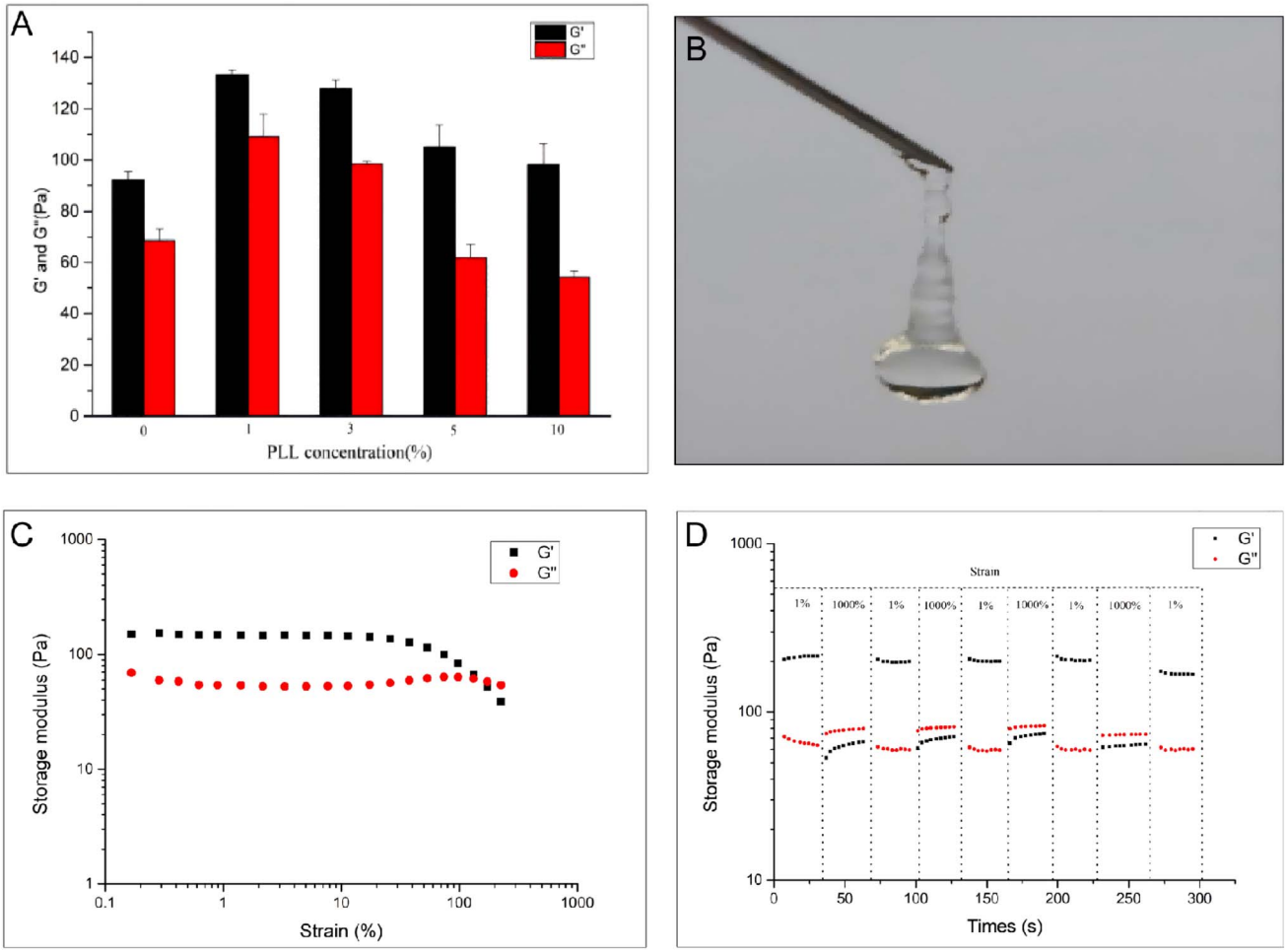

Fig. 1 Experiments on the injectable properties of HAG/PLL hydrogels. (A) Modulus of injectable antimicrobial HAG/PLL hydrogel with different PLL contents; (B) state of the hydrogel passing through a 26 G injection needle; (C) strain rate amplitude of injectable antimicrobial hydrogel HAG/PLL from 0.1 to 1000% at a fixed temperature of 37 °C and a frequency set at 1 Hz scanning test; (D) thixotropy experiment of injectable antimicrobial hydrogel HAG/PLL by continuous conversion of strain rate at a fixed temperature of 37 °C.

process where cross-linking points continuously form and dissociate. The results confirm that the HAG/PLL hydrogel possesses self-healing capabilities. This attribute ensures that the HAG/PLL hydrogel is malleable during application and can be manually kneaded to uniformly fill the entire pocket.

3.2 Morphology of the hydrogels

As anticipated, the interface of the freeze-dried HAG-PLL hydrogel observed through SEM differed from that of the HAG hydrogel. The HAG hydrogel (Fig. 2A) exhibits a layered, flaky structure, which appeared smooth at higher magnifications. In contrast, the HAG-PLL hydrogel (Fig. 2B) displayed an interconnected three-dimensional (3D) porous microstructure. Magnification depicted that the surface adsorbed solid materials, likely ascribed to the electrostatic interactions between the amine groups on PLL and the carboxyl groups on HAG. This could account for the observed increase in the storage modulus (G') of the HAG/PLL hydrogel upon the introduction of PLL.

3.3 *In vitro* PLL release

The antimicrobial efficacy of HAG/PLL hydrogels is largely dependent on PLL. Therefore, it is crucial to detect the PLL release of HAG/PLL hydrogels *in vitro*. As depicted in Fig. 3, at pH 7.4, the hydrogel exhibited a sustained release pattern, with approximately 79% of PLL being released within the 1st day and around 91% by the 4th day, followed by a gradual release, in line with the desired therapeutic strategy of delivering a substantial amount of PLL immediately postoperatively to combat potential pathogens, while the subsequent slower release phase acts as a prophylaxis.[7,50,51] Furthermore, the sustained release duration can extend up to approximately 18 days, corresponding with the natural healing timeline of human tissues. Experimental data showed that the release rate and cumulative daily release of PLL at pH 5.0 were higher than those at pH 7.4. Given that the microenvironment of infected wounds is typically acidic (pH 5.5–6.5), this pH responsive characteristic can precisely promote the rapid release of PLL, thereby enhancing local antibacterial efficacy. Taken together, the findings implied the release profile of the hydrogel was satisfactory.

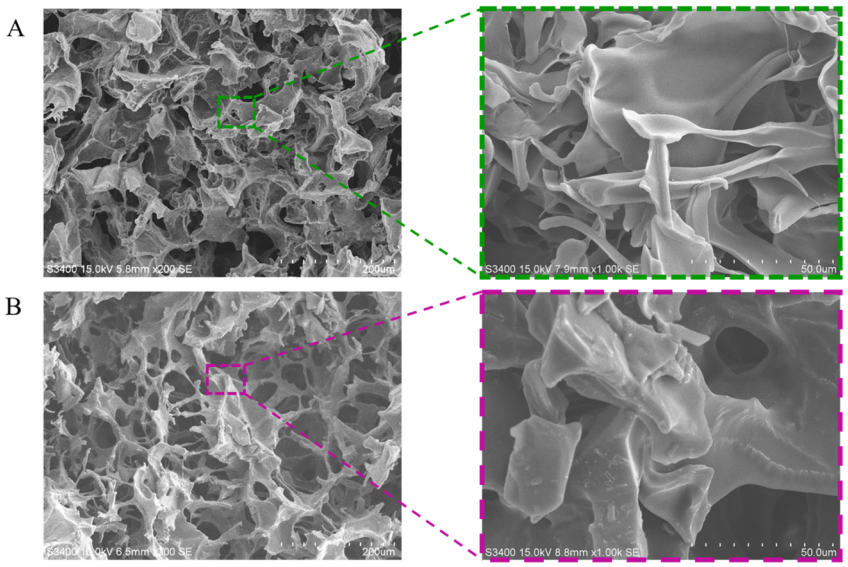

Fig. 2 SEM images of. (A) HAG hydrogel, (B) HAG/PLL hydrogel.

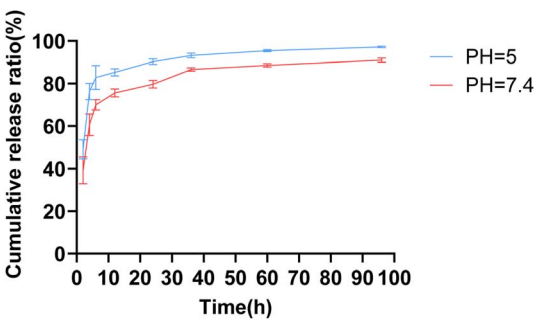

Fig. 3 The cumulative release of PLL from HAG/PLL hydrogel in different pH.

3.4 Biocompatibility assay

Biomaterials are foreign to the host and are bound to elicit response or rejection in the body after implantation.[52] Therefore, excellent biomaterials must possess outstanding biocompatibility so that the response is acceptable and not detrimental to the host. While *in vitro* safety evaluation is generally excellent owing to its simplicity, shorter duration, and high reproducibility, simulating the complex environment in *vivo* poses challenges. Conversely, in *vivo* safety evaluation can better reflect the behavior of biomaterials after implantation but can only observe specific time points rather than the whole implantation process. Therefore, the combination of *in vivo* and *ex vivo* safety can better reflect the impact of biomaterials on the organism and their overall safety.

The results of CCK8 cell viability assay and cell live-dead staining demonstrated that HAG/PLL hydrogels had excellent cytocompatibility. Noteworthily, cell viability is an indicator of cytotoxicity, with cell viability >80% representing non-toxicity. As shown in Fig. 4A, the effect of PLL concentration on cell viability was investigated. The results show that noticeable cytotoxicity occurs only when the PLL concentration reaches 10 wt%. In our HAG/PLL hydrogel system, the PLL content is maintained at 5 wt%, which further confirms the favorable biocompatibility of the hydrogel. As delineated in Fig. 4B, the HAG/PLL hydrogel group did not induce significant cytotoxicity compared to the control group, with cell survival rates >100% on both days 1 and 3. As shown in Fig. 4C–E, the hemolysis assay unveiled that the hemolysis rate marginally decreased with an increase in PLL content and was below 5%. This meets the acceptance criteria of ISO 10993-4.[36,53] At the same time, microscopic examination displayed that the hemoglobin in the positive experimental group was basically dissolved, whereas no such changes were noted in the negative control and HAG/PLL hydrogel groups, suggesting that HAG/PLL hydrogel did not damage red blood cells and possessed excellent blood compatibility. As presented in Fig. 4F, green fluorescence was observed in both the control and HAG/PLL hydrogel groups, with no significant difference in cell morphology, indicating the absence of significant cytotoxicity in the co-culture of the hydrogel extract with L929 cells. Given that HA and PLL are metabolized by the liver and kidneys, liver and kidney function tests were conducted to evaluate the impact of the hydrogel on these functions. At the same time, hematological tests, including C-reactive protein (CRP) levels, were performed, and skin, myocardial, liver, and kidney tissues were harvested from the injection area for hematoxylin and eosin (HE) staining to comprehensively evaluate the *in vivo* safety of the HAG/PLL hydrogel. As shown in Fig. 4G, HE staining of the tissues surrounding the injection site, as well as myocardial, liver, and kidney tissues, revealed no significant inflammatory cell infiltration. Additionally, there were no noticeable changes in tissue architecture. As depicted in Fig. 4H, the levels of alanine aminotransferase (ALT), glutamate aminotransferase (AST), urea nitrogen (BUN), serum creatinine (CREA), and C-reactive protein (CRP) were comparable between the control and experimental groups on the 7th and 30th days post-hydrogel implantation (Fig. S1). These findings collectively imply that

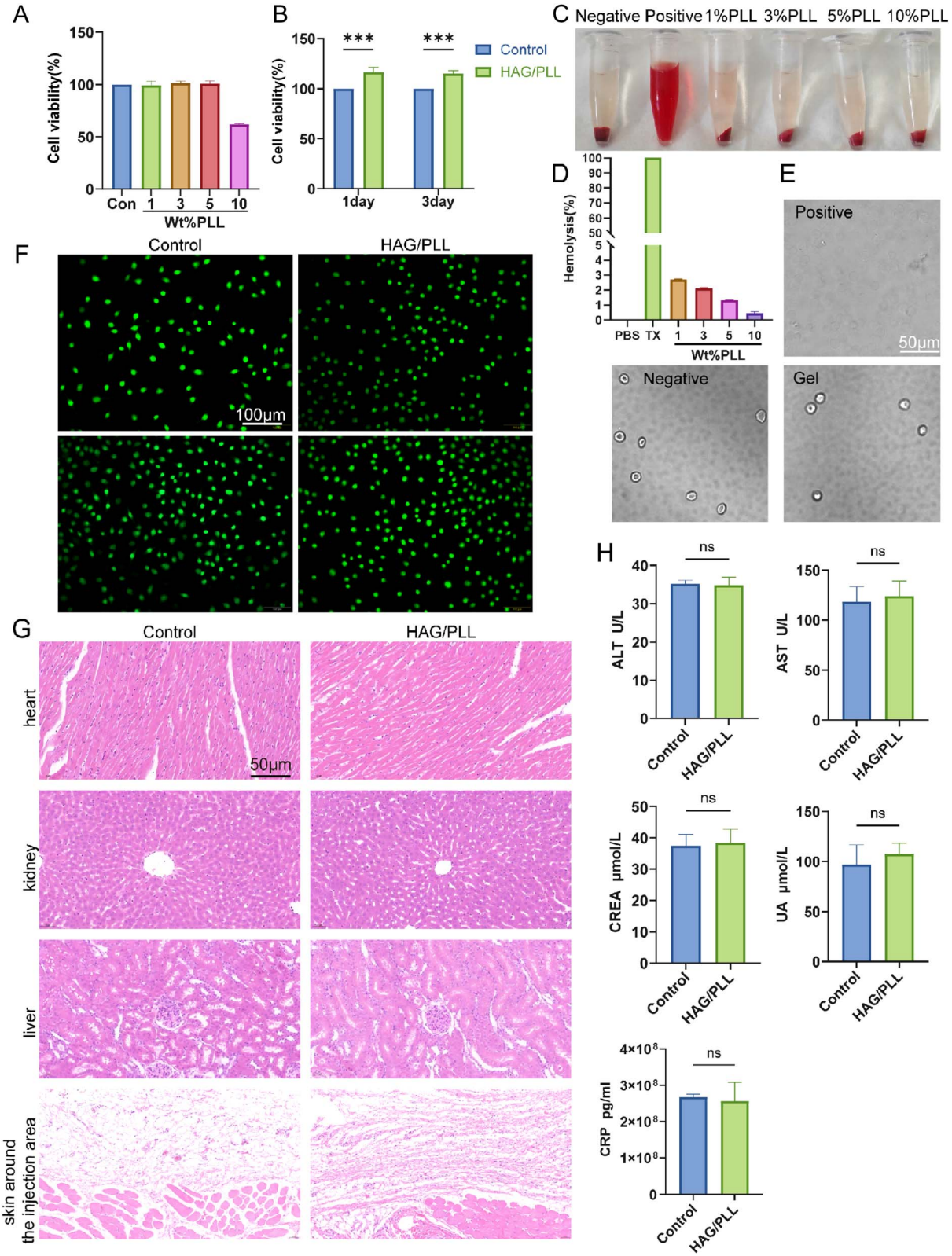

Fig. 4 Biocompatibility assay. (A) Cell viability curves of cells treated with different concentrations of PLL; (B) cytotoxicity evaluation ($n = 3$); *In vitro* hemocompatibility assay of HAG/PLL antimicrobial hydrogel: (C) Physical pictures of red blood cell hemolysis; (D) HAG/PLL hydrogel hemolysis rate at different concentrations of PLL (PBS was the negative control and Triton x-100 was the positive control); (E) erythrocyte compatibility assay; (F) cell live-dead staining; (G) HE staining of the control group and the HAG/PLL group on 7th day HE staining; (H) blood biochemical levels (CRP, liver, kidney function) in control group and HAG/PLL group on 7th day ($n = 3$), $P \geq 0.05$.

the HAG/PLL hydrogel did not induce significant toxicity or provoke an inflammatory response. Additionally, we injected hydrogels of FITC-labeled HAG-PLL into a dorsal subcutaneous pouch in rat. At regular intervals, the *in vivo* retention of the hydrogels was observed under ultraviolet light. As shown in the Fig. S2, the hydrogel was almost completely degraded around day 25.

3.5 Evaluation of antimicrobial performance

At present, antibiotic resistance is a growing issue due to antibiotic abuse and continuous microbial mutation.[54] Therefore, non-antibiotic materials with antimicrobial properties were used to address CIED-associated infections.

3.5.1 *In vitro* antimicrobial evaluation. Herein, the *in vitro* antimicrobial properties of HAG/PLL hydrogel were evaluated by the hydrogel ring of inhibition test, colony counting assay, and live/dead bacterial fluorescent staining.

The hydrogel inhibition test exposed (Fig. 5A–D) that the antimicrobial activity of the hydrogel steadily increased with an increase in PLL content. However, to maintain the modulus of the hydrogel, the content of PLL was not continuously increased to enhance its antimicrobial effect. For further comparison, the

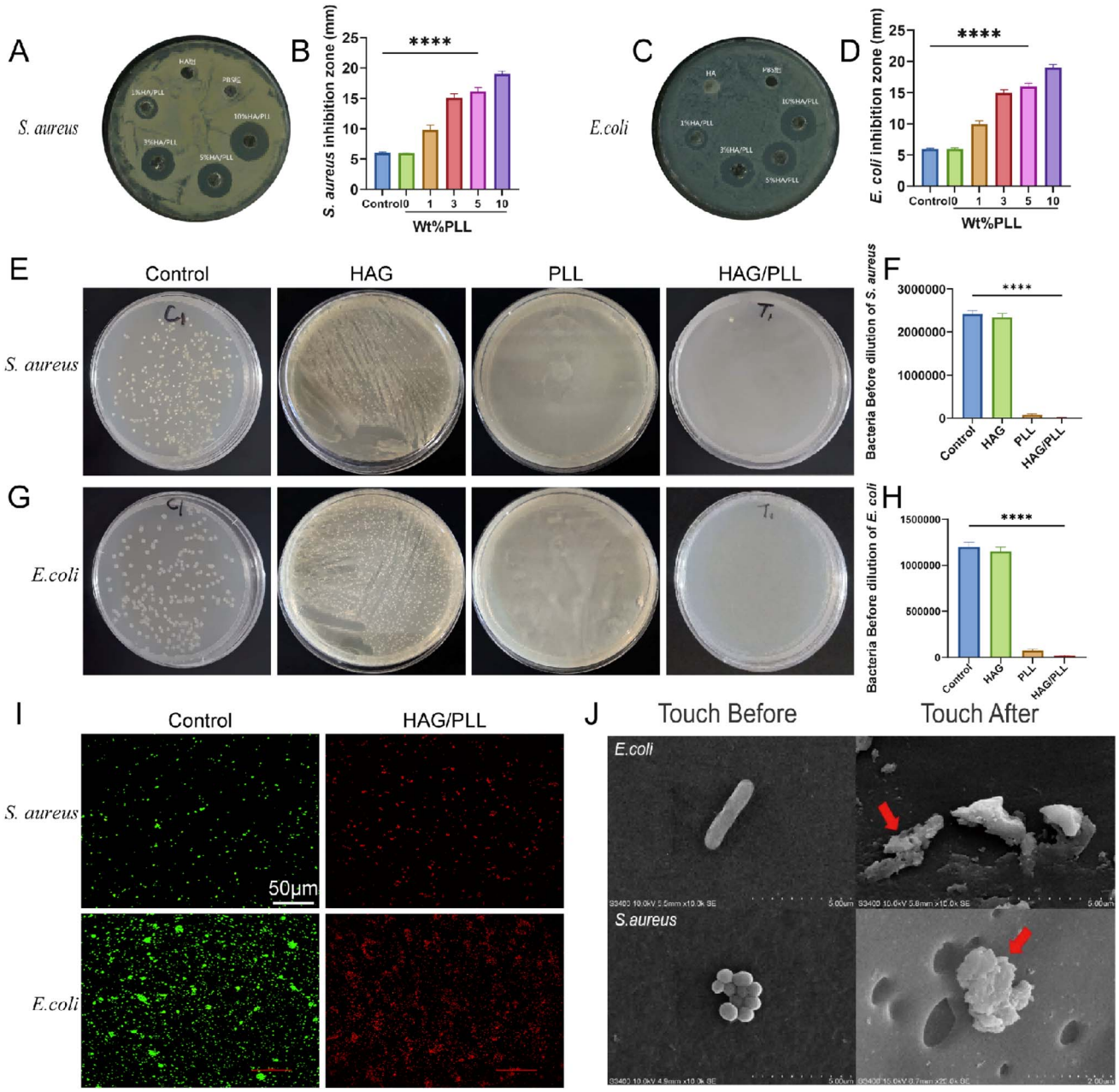

Fig. 5 HAG/PLL hydrogel circle of inhibition assay. (A and B) *S. aureus* circle of inhibition size and its statistical graph ($n = 3$); (C and D) *E. coli* circle of inhibition size and its statistical graph ($n = 3$); (E–H) colony counts ($n = 3$); (I) staining of live-dead bacteria; (J) bacterial morphology on the surface of the HAG/PLL hydrogel (*E. coli* and *S. aureus*).

antimicrobial performance of HAG hydrogel alone, PLL solution alone, and the composite HAG/PLL hydrogel itself are directly contrasted in Fig. S3, highlighting the synergistic contribution of PLL within the hydrogel system.

After co-culturing the HAG/PLL hydrogel extract with representative CIED infection pathogens, namely G^- (*E. coli*) and G^+ (*S. aureus*), for 24 h, colonies were counted and compared. As shown in Fig. 5E–H, the control group was densely populated with colonies, indicating that a large number of *S. aureus* and *E. coli* survived, while colonies were occasionally observed in the HAG/PLL hydrogel group, and the difference was statistically significant (P value < 0.0001), signaling that the HAG/PLL hydrogel possessed excellent *in vitro* antibacterial properties. The *in vitro* antimicrobial activity of HAG/PLL hydrogels was further evaluated by live/dead bacterial staining. As shown in Fig. 5I, live and dead bacteria were stained green and red, respectively. The results revealed that the HAG/PLL hydrogel group exclusively emitted red fluorescence, which indicated that the majority of bacteria were killed after 1 h of co-cultivation, reflecting its favorable antibacterial performance.

In addition, the morphology of bacteria (*S. aureus* and *E. coli*) was observed after co-culturing with the HAG/PLL hydrogel using SEM. As illustrated in Fig. 5J, the cell walls of *S. aureus* and *E. coli* were wrinkled and perforated after contact with the HAG/PLL hydrogel, thus validating the antimicrobial properties of the HAG/PLL hydrogel.

3.5.2 *In vivo* antimicrobial evaluation. To simulate CIED infection, a pacemaker was implanted in the back of New Zealand rabbits. The pocket was opened and observed on the 7th day after implantation. The Fig. 6A showed the general diagram of pacemaker pocket infection in male New Zealand rabbits. As shown in Fig. 6B, considering that the bacterial load injected exceeded that of clinical infection and the implanted pacemaker was a foreign body, a secretion indicative of inflammatory reaction was detected in all groups. However, the amount of pus in the pocket in the hydrogel group was significantly reduced compared with the model group, and the inflammatory reaction and infection degree were significantly reduced, but there was no significant difference with the RFP group, indicating that HAG/PLL hydrogel had significant antibacterial effect on bag infection. To further evaluate the antibacterial effect of hydrogel on bag infection, we collected the peripheral blood of experimental rabbits, and measured the total number of white blood cells and neutrophils. As shown in Fig. S4, the level of inflammatory cells in the model group significantly increased, indicating that infection triggered a systemic inflammatory response. Although the inflammatory indicators in the treatment group decreased, there was no statistically significant difference compared to the model group, indicating that the impact of local pocket infection on systemic inflammatory response is relatively limited. In addition, there is no significant difference in inflammatory cell level between the hydrogel group and the rifampicin group, suggesting that hydrogel has certain antibacterial activity in controlling local infection, but its systemic anti-inflammatory effect may be limited by the local infection focus and the low-level diffusion of inflammatory mediators. Besides, the antimicrobial activity of the HAG/PLL hydrogel was assessed through bacterial live-dead staining and HE staining of tissues around the pocket. As shown in Fig. 6C, the difference between green and red fluorescence was not significant on the surface of the pacemaker in the model group, whereas the red fluorescence intensity on the surface of the pacemaker in the HAG/PLL hydrogel group and RFP group was significantly higher than the green fluorescence intensity, indicating the presence of a large number of dead *S. aureus*. Meanwhile, the HE staining results (shown in Fig. 6D) revealed a large number of neutrophils in the mucous membrane of the muscle tissues of the model group and a significantly lower infiltration level of neutrophils in the HAG/PLL group and RFP group. To further compare the inflammatory response, the levels of inflammatory factors around the pocket were measured. The results of the immunohistochemical assay showed (shown in Fig. 6E) that the levels of the inflammatory factors IL-β and TNF-α were significantly higher in the model group compared to the HAG/PLL group. In conclusion, our results demonstrated that the HAG/PLL hydrogel possessed potent anti-inflammatory and antimicrobial properties, which can effectively prevent pocket infection.

3.6 Antimicrobial mechanism of HAG/PLL hydrogels

Herein, SEM displayed that *S. aureus* and *E. coli* had folds and perforations in their cell walls after exposure to HAG/PLL hydrogels. Therefore, we speculate that the primary mechanism underlying the antibacterial activity of HAG/PLL hydrogels involves the disruption of the integrity of the bacterial cell wall. To further explore the antibacterial mechanism of HAG/PLL hydrogels, bacterial reactive oxygen species and MDA levels were measured, and a biofilm formation assessment was conducted. As shown in Fig. 7A, after treating the bacterial solution with HAG/PLL hydrogel extract and PBS for 24 h, minimal green fluorescence was observed in the control group, whereas significant green fluorescence was observed in the HAG/PLL group, suggesting that treatment with HAG/PLL hydrogel extract for 24 h promoted ROS generation in bacteria. Besides, the ROS level in NAC group is significantly reduced compared with that in HAG/PLL group, indicating the role of ROS in the sterilization of HAG/PLL hydrogel. Regarding the biofilm formation, as shown in Fig. 7B, no significant biofilm formation was noted in the hydrogel group, whereas intact biofilms were observed for both *S. aureus* and *E. coli*. In summary, the specific antibacterial mechanism of HAG/PLL hydrogel involves its bactericidal effects by stimulating bacteria to produce excessive ROS upon contact, which subsequently attacks the lipids on the bacterial cell membranes, eventually culminating in lipid peroxidation, bacterial cell membrane destruction, and the loss of bacterial integrity.[26] In addition, the HAG/PLL hydrogels exert antimicrobial effects by inhibiting bacterial biofilm formation to limit the activity and pathogenicity of bacteria. As shown in Fig. 7C, the level of MDA, the end product of lipid peroxidation,[55–57] was markedly higher in the HAG/PLL hydrogel group compared to the control group (P < 0.0005).

We adopted the strategy of "BDDE covalent micro gel blocking": firstly, HAG was prepared by crosslinking BDDE,

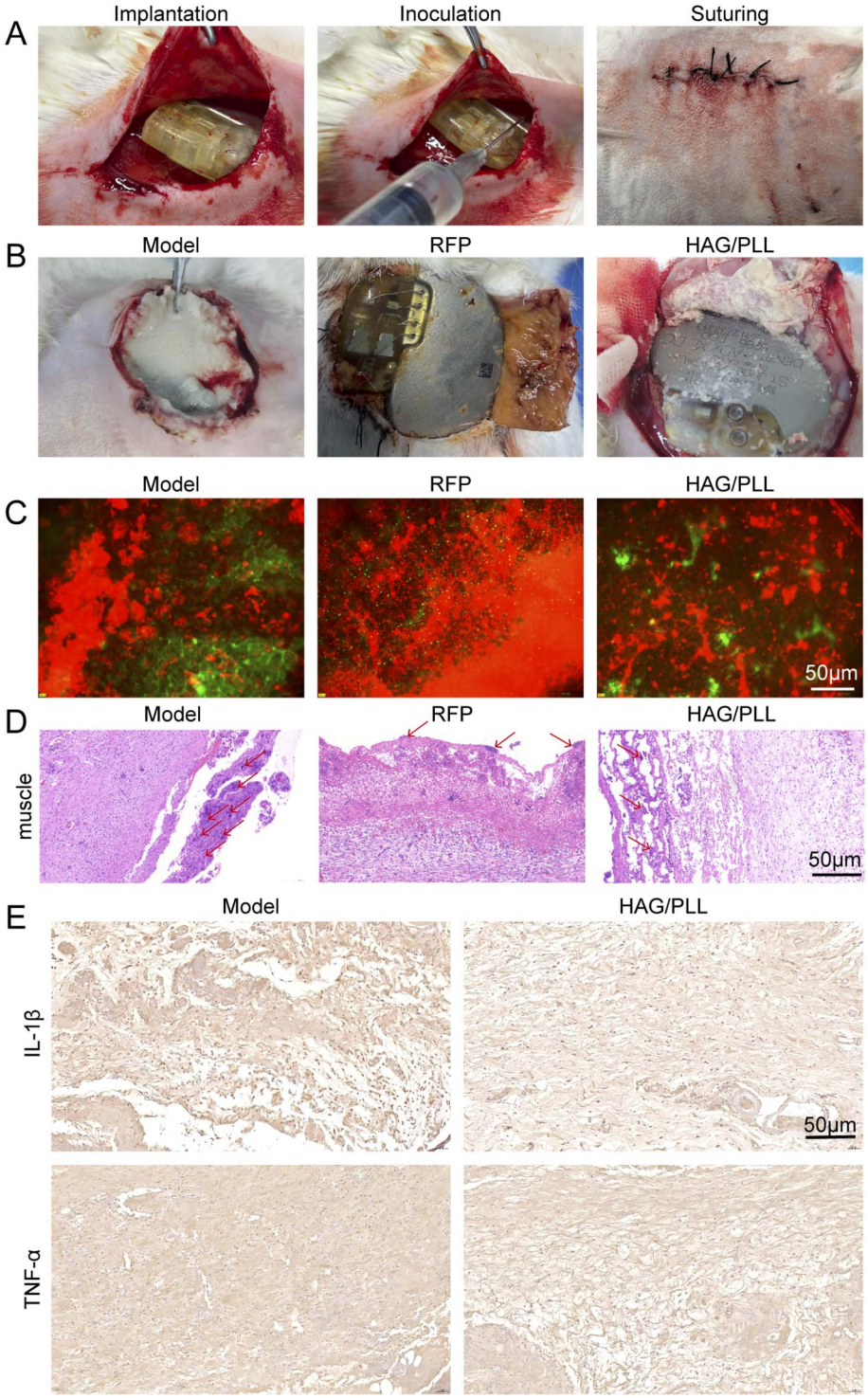

Fig. 6 *In vivo* antimicrobial evaluation. (A) General diagram of pacemaker pocket infection in male New Zealand rabbits; (B) pocket infection status in each group 7 days postoperatively; (C) staining of live dead bacteria; (D) HE staining of muscle tissue around the pocket: the red arrow indicates inflammatory cell infiltration; (E) detection of inflammatory factors in the surrounding tissue of the pocket by immunohistochemistry (IL-β, TNF-α).

which significantly increased the specific surface area; subsequently, excess ε-PLL was anchored through secondary electrostatic adsorption. This strategy not only enhances antibacterial efficacy, but also endows the material with injectable and moldable properties, and presents instantaneous shear recovery ability and stable elastic modulus, which can perfectly fit narrow and irregular CIED bags and intraoperative operation needs. Salma Ancane *et al.*[58] reported that the antibacterial rate of physical cross-linked HA/PLL hydrogel against standard strains exceeded 99.999%, while chemical cross-

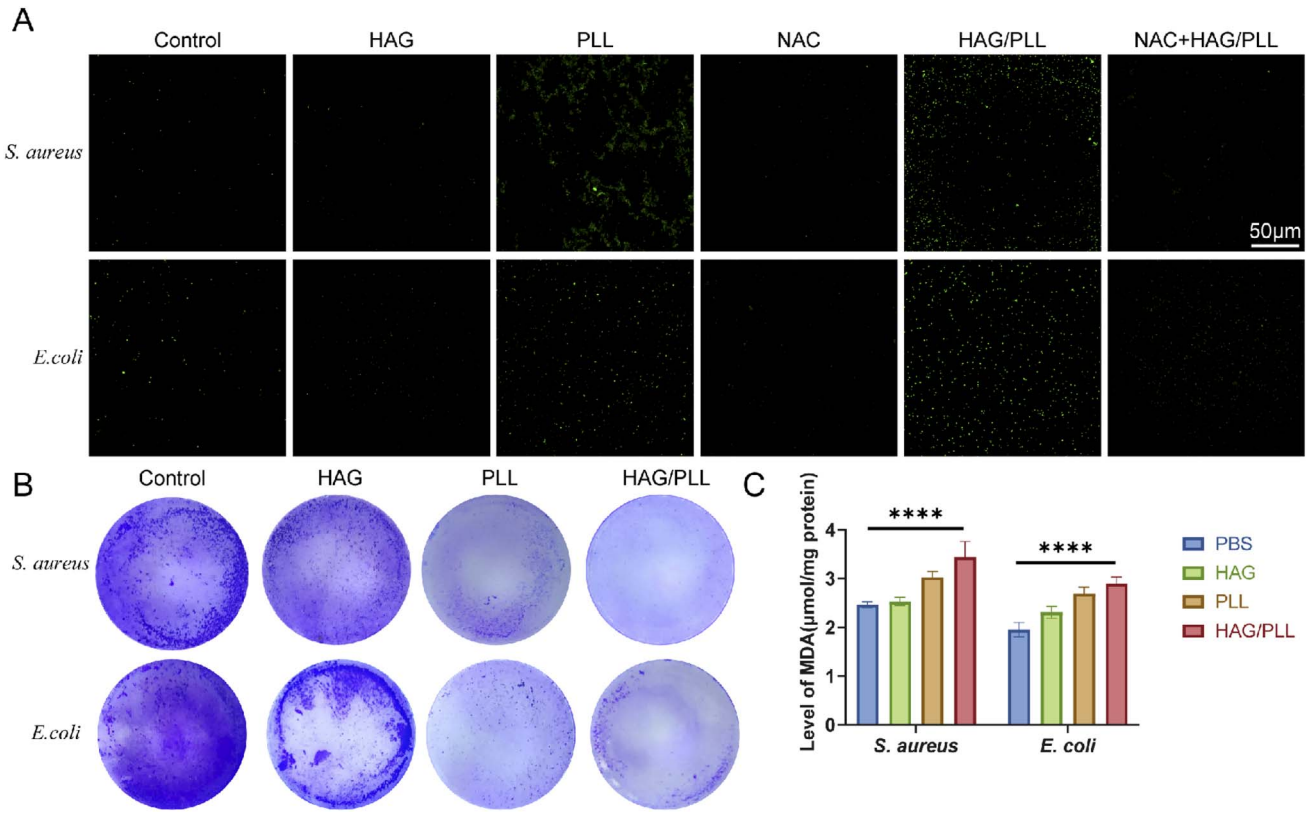

Fig. 7 Antibacterial mechanism. (A) Bacterial reactive oxygen species assay; (B) Biofilm Formation Test of *S. aureus* and *E. coli*; (C) MDA assay ($n = 3$).

linking weakened the antibacterial performance, which directly supported the superiority of our design route. In addition, the existing HA/PLL hydrogel[59–61] focuses on the repair of skin wounds, and there is no system specially developed for the prevention of CIED bag infection. Our HAG/PLL antibacterial hydrogel can be completely degraded within 30 days without obvious cytotoxicity.[62] It is the first time to provide hyaluronic acid based antibacterial injection for implantable cardiac electronic devices, marking a key step for the clinical transformation of HA antibacterial materials.

4. Conclusion

This study developed an injectable and antimicrobial hydrogel based on HA and PLL by leveraging its physical properties and antimicrobial activity. This hydrogel exhibited excellent injectability, self-healing capabilities, and degradability. Additionally, the HAG/PLL hydrogel is not only non-toxic to L929 cells but also demonstrates an erythrocyte hemolysis rate of less than 5%, which is significantly lower than the international standard, highlighting its superior cytocompatibility. In New Zealand rabbit pocket infection models, the HAG/PLL hydrogel significantly eliminated *S. aureus* and alleviated the inflammatory response compared to the control group, demonstrating favorable antimicrobial effects. Furthermore, the experimental results revealed that the HAG/PLL hydrogel effectively targeted representative flora associated with CIED infections by inducing excessive reactive oxygen species (ROS) production in bacteria, which in turn damaged lipids on bacterial cell membranes, resulting in membrane disruption. In summary, the HAG/PLL hydrogel is simple and convenient to prepare, possesses satisfactory biological safety, and exhibits outstanding antibacterial activity. It shows promise in preventing CIED pocket infections and is anticipated to offer new perspectives and solutions for addressing challenges related to CIED infections.

Author contributions

Jin-e Liu: investigation, resources, validation, writing original draft. Zikang Cheng: investigation, resources, validation. Peixu Zhao: investigation. Yanfei Wu: investigation. Lingjuan Zhu: supervision. Chao Yu: investigation, resources. Wei Zhou: supervision. Tao Wang: supervision. Xiaoshu Cheng: resources, supervision. Quanbin Dong: project administration, writing – review & editing. Huihui Bao: project administration, data curation, funding acquisition, writing – original draft, writing – review & editing.

Conflicts of interest

The authors declare that they have no known competing financial interests or personal relationships that could influence the work reported in this paper.

Data availability

Data will be made available on request.

Acknowledgements

This work was supported by the National Natural Science Foundation of China (82260168, 82160070, 82460670).

References

1 R. Duncan and M. J. Vicent, Polymer therapeutics-prospects for 21st century: the end of the beginning, *Adv. Drug Delivery Rev.*, 2013, **65**, 60–70.
2 V. K. Phadke, D. S. Hirsh and N. D. Goswami, Patient Report and Review of Rapidly Growing Mycobacterial Infection after Cardiac Device Implantation, *Emerging Infect. Dis.*, 2016, **22**, 389–395.
3 C. J. Arnold and V. H. Chu, Cardiovascular Implantable Electronic Device Infections, *Infect. Dis. Clin. N. Am.*, 2018, **32**, 811–825.
4 L. M. Baddour, *et al.*, Update on Cardiovascular Implantable Electronic Device Infections and Their Prevention, Diagnosis, and Management: A Scientific Statement From the American Heart Association: Endorsed by the International Society for Cardiovascular Infectious Diseases, *Circulation*, 2024, **149**, e201–e216.
5 J. C. Diaz, *et al.*, Chlorhexidine gluconate pocket lavage to prevent cardiac implantable electronic device infection in high-risk procedures, *Heart Rhythm*, 2023, **20**, 1674–1681.
6 M. H. J. P. Frausing, M. B. Kronborg, J. B. Johansen and J. C. Nielsen, Avoiding implant complications in cardiac implantable electronic devices: what works?, *Europace*, 2021, **23**, 163–173.
7 C. Blomström-Lundqvist, *et al.*, European Heart Rhythm Association (EHRA) international consensus document on how to prevent, diagnose, and treat cardiac implantable electronic device infections-endorsed by the Heart Rhythm Society (HRS), the Asia Pacific Heart Rhythm Society (APHRS), the Latin American Heart Rhythm Society (LAHRS), International Society for Cardiovascular Infectious Diseases (ISCVID) and the European Society of Clinical Microbiology and Infectious Diseases (ESCMID) in collaboration with the European Association for Cardio-Thoracic Surgery (EACTS), *Europace*, 2020, **22**, 515–549.
8 V. Traykov, *et al.*, Clinical practice and implementation of guidelines for the prevention, diagnosis and management of cardiac implantable electronic device infections: results of a worldwide survey under the auspices of the European Heart Rhythm Association, *Europace*, 2019, **21**, 1270–1279.
9 A. Polewczyk, W. Jacheć, L. Segreti, M. G. Bongiorni and A. Kutarski, Influence of the type of pathogen on the clinical course of infectious complications related to cardiac implantable electronic devices, *Sci. Rep.*, 2021, **11**, 14864.
10 C. Lennerz, *et al.*, Biomarker-based diagnosis of pacemaker and implantable cardioverter defibrillator pocket infections: A prospective, multicentre, case-control evaluation, *PLoS One*, 2017, **12**, e0172384.
11 M. G. Bongiorni, *et al.*, How European centres diagnose, treat, and prevent CIED infections: results of an European Heart Rhythm Association survey, *Europace*, 2012, **14**, 1666–1669.
12 S. Mittal, *et al.*, Cardiac implantable electronic device infections: incidence, risk factors, and the effect of the AigisRx antibacterial envelope, *Heart Rhythm*, 2014, **11**, 595–601.
13 C. A. Henrikson, *et al.*, Antibacterial Envelope Is Associated With Low Infection Rates After Implantable Cardioverter-Defibrillator and Cardiac Resynchronization Therapy Device Replacement: Results of the Citadel and Centurion Studies, *JACC Clin Electrophysiol*, 2017, **3**, 1158–1167.
14 H. L. Bloom, *et al.*, Implantation success and infection in cardiovascular implantable electronic device procedures utilizing an antibacterial envelope, *PACE-Pacing Clin. Electrophysiol.*, 2011, **34**, 133–142.
15 L. K. Hansen, *et al.*, In vivo model of human pathogen infection and demonstration of efficacy by an antimicrobial pouch for pacing devices, *PACE-Pacing Clin. Electrophysiol.*, 2009, **32**, 898–907.
16 L. K. Hansen, K. Berg, D. Johnson, M. Sanders and M. Citron, Efficacy of local rifampin/minocycline delivery (AIGIS(RX)®) to eliminate biofilm formation on implanted pacing devices in a rabbit model, *Int. J. Artif. Organs*, 2010, **33**, 627–635.
17 D. Schwartzman, *et al.*, An off-the-shelf plasma-based material to prevent pacemaker pocket infection, *Biomaterials*, 2015, **60**, 1–8.
18 W. Eisenreich, T. Rudel, J. Heesemann and W. Goebel, Link Between Antibiotic Persistence and Antibiotic Resistance in Bacterial Pathogens, *Front Cell Infect Microbiol*, 2022, **12**, 900848.
19 V. Gribova, *et al.*, Polyarginine as a Simultaneous Antimicrobial, Immunomodulatory, and miRNA Delivery Agent within Polyanionic Hydrogel, *Macromol. Biosci.*, 2022, **22**, e2200043.
20 S.-J. Liu and S.-C. Liao, Surface Modification of Bamboo Charcoal by O2 Plasma Treatment and UV-Grafted Thermo-Sensitive AgNPs Hydrogel to Improve Antibacterial Properties in Biomedical Application, *Nanomaterials*, 2021, **11**, 2697.
21 Y. Ren, *et al.*, Mussel-Inspired Carboxymethyl Chitosan Hydrogel Coating of Titanium Alloy with Antibacterial and Bioactive Properties, *Materials*, 2021, **14**, 6901.
22 S. Ghosh, S. Mukherjee, D. Patra and J. Haldar, Polymeric Biomaterials for Prevention and Therapeutic Intervention of Microbial Infections, *Biomacromolecules*, 2022, **23**, 592–608.
23 W. Liao, *et al.*, Physicochemical, antibacterial and food preservation properties of active packaging films based on chitosan/ε-polylysine-grafted bacterial cellulose, *Int. J. Biol. Macromol.*, 2023, **253**, 127231.
24 S. Karthick Raja Namasivayam, A. John, R. S. Arvind Bharani, M. Kavisri, M. Kavisri and M. Moovendhan, Biocompatible formulation of cationic antimicrobial peptide Polylysine

(PL) through nanotechnology principles and its potential role in food preservation - A review, *Int. J. Biol. Macromol.*, 2022, **222**, 1734–1746.

25 S. Pourshahrestani, E. Zeimaran and M. B. Fauzi, Antibacterial polylysine-containing hydrogels for hemostatic and wound healing applications: preparation methods, current advances and future perspectives, *Biomater. Sci.*, 2024, **12**, 3293–3320.

26 M. Hyldgaard, *et al.*, The antimicrobial mechanism of action of epsilon-poly-l-lysine, *Appl. Environ. Microbiol.*, 2014, **80**, 7758–7770.

27 Y. Meng, *et al.*, Antibacterial Activity and Mechanism of Action of Whey Protein-ε-Polylysine Complexes against Staphylococcus aureus and Bacillus subtilis, *Foods*, 2022, **11**, 2311.

28 Z. Shao, *et al.*, Mechanism of the antimicrobial activity of whey protein-ε-polylysine complexes against Escherichia coli and its application in sauced duck products, *Int. J. Food Microbiol.*, 2020, **328**, 108663.

29 T. Yoshida and T. Nagasawa, ε-Poly-l-lysine: microbial production, biodegradation and application potential, *Appl. Microbiol. Biotechnol.*, 2003, **62**, 21–26.

30 H. Zhang, S. Huang, X. Yang and G. Zhai, Current research on hyaluronic acid-drug bioconjugates, *Eur. J. Med. Chem.*, 2014, **86**, 310–317.

31 M. F. P. Graça, S. P. Miguel, C. S. D. Cabral and I. J. Correia, Hyaluronic acid-Based wound dressings: A review, *Carbohydr. Polym.*, 2020, **241**, 116364.

32 Y. Lan, A modified hyaluronic acid hydrogel with strong bacterial capture and killing capabilities for drug-resistant bacteria-infected diabetic wound healing, *Int. J. Biol. Macromol.*, 2024.

33 H. Chen, Z. Fang, M. Song and K. Liu, Mitochondrial targeted hierarchical drug delivery system based on HA-modified liposomes for cancer therapy, *Eur. J. Med. Chem.*, 2022, **241**, 114648.

34 A. Marinho, C. Nunes and S. Reis, Hyaluronic Acid: A Key Ingredient in the Therapy of Inflammation, *Biomolecules*, 2021, **11**, 1518.

35 M. G. Neuman, R. M. Nanau, L. Oruña-Sanchez and G. Coto, Hyaluronic acid and wound healing, *J. Pharm. Pharm. Sci.*, 2015, **18**, 53–60.

36 M. Zhang, *et al.*, Multifunctional Nanocomposites for Targeted, Photothermal, and Chemotherapy, *Chem. Mater.*, 2019, **31**, 1847–1859.

37 B. Nyström, *et al.*, Characterization of polyelectrolyte features in polysaccharide systems and mucin, *Adv. Colloid Interface Sci.*, 2010, **158**, 108–118.

38 P. M. Wolny, *et al.*, Analysis of CD44-hyaluronan interactions in an artificial membrane system: insights into the distinct binding properties of high and low molecular weight hyaluronan, *J. Biol. Chem.*, 2010, **285**, 30170–30180.

39 A. G. Tavianatou, *et al.*, Hyaluronan: molecular size-dependent signaling and biological functions in inflammation and cancer, *FEBS J.*, 2019, **286**, 2883–2908.

40 Y. Liu, *et al.*, Bio-inspired, bio-degradable adenosine 5'-diphosphate-modified hyaluronic acid coordinated hydrophobic undecanal-modified chitosan for hemostasis and wound healing, *Bioact Mater*, 2022, **17**, 162–177.

41 Y. Liu, *et al.*, Bioactive Phenylboronic Acid-Functionalized Hyaluronic Acid Hydrogels Induce Chondro-Aggregates and Promote Chondrocyte Phenotype, *Macromol. Biosci.*, 2023, **23**, e2300153.

42 S. P. Miguel, D. Simões, A. F. Moreira, R. S. Sequeira and I. J. Correia, Production and characterization of electrospun silk fibroin based asymmetric membranes for wound dressing applications, *Int. J. Biol. Macromol.*, 2019, **121**, 524–535.

43 G. D. Monheit and K. M. Coleman, Hyaluronic acid fillers, *Dermatol. Ther.*, 2006, **19**, 141–150.

44 Z. Erisgin, *et al.*, Use of hyaluronic acid matrix in dorsal augmentation rhinoplasty, *Biotech. Histochem.*, 2023, **98**, 561–566.

45 X. Huang, *et al.*, Peptide hydrogel platform encapsulating manganese ions and high-density lipoprotein nanoparticle-mimicking nanovaccines for the prevention and treatment of gastric cancer, *J. Transl. Med.*, 2025, **23**, 371.

46 X. Sun, H. Ding, X. Li, Y. Wu and X. Huang, Disulfiram-loaded nanovesicles hydrogel promotes healing of diabetic wound, *J. Transl. Med.*, 2024, **22**, 1066.

47 P. M. Arvejeh, *et al.*, A novel approach for the co-delivery of 5-fluorouracil and everolimus for breast cancer combination therapy: stimuli-responsive chitosan hydrogel embedded with mesoporous silica nanoparticles, *J. Transl. Med.*, 2025, **23**, 382.

48 B. Zhang, *et al.*, Injectable nanocomposite hydrogel for localized precision delivery of dexamethasone after traumatic brain injury: dual modulation of neuroinflammation and blood–brain barrier restoration, *J. Transl. Med.*, 2025, **23**, 579.

49 Q. Dong, *et al.*, Hyaluronic acid-based antibacterial hydrogels constructed by a hybrid crosslinking strategy for pacemaker pocket infection prevention, *Carbohydr. Polym.*, 2020, **245**, 116525.

50 N. O. Palmeri, D. B. Kramer, A. W. Karchmer and P. J. Zimetbaum, A Review of Cardiac Implantable Electronic Device Infections for the Practicing Electrophysiologist, *JACC Clin Electrophysiol*, 2021, **7**, 811–824.

51 Y. Xiong, *et al.*, Light-sensitive PEG hydrogel with antibacterial performance for pacemaker pocket infection prevention, *Mater. Today Bio*, 2024, **25**, 100987.

52 Y. Ramot, M. Haim-Zada, A. J. Domb and A. Nyska, Biocompatibility and safety of PLA and its copolymers, *Adv. Drug Delivery Rev.*, 2016, **107**, 153–162.

53 M. Zhang, *et al.*, pH-Sensitive N-doped carbon dots–heparin and doxorubicin drug delivery system: preparation and anticancer research, *RSC Adv.*, 2017, **7**, 9347–9356.

54 M. Huemer, S. Mairpady Shambat, S. D. Brugger and A. S. Zinkernagel, Antibiotic resistance and persistence-Implications for human health and treatment perspectives, *EMBO Rep.*, 2020, **21**, e51034.

55 T. T. Nguyen, L. Q. Ngo, A. Promsudthi and R. Surarit, Salivary Lipid Peroxidation in Patients With Generalized

Chronic Periodontitis and Acute Coronary Syndrome, *J Periodontol*, 2016, **87**, 134–141.

56 L. F. Dmitriev and V. N. Titov, Lipid peroxidation in relation to ageing and the role of endogenous aldehydes in diabetes and other age-related diseases, *Ageing Res Rev*, 2010, **9**, 200–210.

57 D. Tsikas, Assessment of lipid peroxidation by measuring malondialdehyde (MDA) and relatives in biological samples: Analytical and biological challenges, *Anal. Biochem.*, 2017, **524**, 13–30.

58 K. Salma-Ancane, *et al.*, Effect of crosslinking strategy on the biological, antibacterial and physicochemical performance of hyaluronic acid and ε-polylysine based hydrogels, *Int. J. Biol. Macromol.*, 2022, **208**.

59 S. Liu, *et al.*, Mussel-Inspired Dual-Cross-linking Hyaluronic Acid/ε-Polylysine Hydrogel with Self-Healing and Antibacterial Properties for Wound Healing, *ACS Appl. Mater. Interfaces*, 2020, **12**, 27876–27888.

60 A. Sceglovs, *et al.*, Injectable ε-Polylysine/Hyaluronic Acid Hydrogels with Resistance-Preventing Antibacterial Activity for Treating Wound Infections, *ACS Appl Bio Mater*, 2025, **8**, 9916–9930.

61 N. Sun, *et al.*, Composite Hydrogels with Rapid Self-Healing, Stretchable, Moldable and Antibacterial Properties Based on PVA/ε-Poly-l-lysine/Hyaluronic Acid, *Molecules*, 2024, **29**, 4666.

62 K. Aunina, *et al.*, Exploring the Interplay of Antimicrobial Properties and Cellular Response in Physically Crosslinked Hyaluronic Acid/ε-Polylysine Hydrogels, *Polymers*, 2023, **15**, 1915.